IEEE Access
Multidisciplinary | Rapid Review | Open Access Journal

Received August 30, 2021, accepted October 8, 2021, date of publication October 13, 2021, date of current version October 22, 2021.

Digital Object Identifier 10.1109/ACCESS.2021.3119566

Reconstructed Current Model Predictive Control of NPC Three-Level Grid-Tied Converter With Current Sensor Fault

HUI LI[1], HAN XIAO[1], AND GUANGLU YANG[1,2]
[1]School of Electrical and Information Engineering, Zhengzhou University of Light Industry, Zhengzhou 450002, China
[2]Nanyang Cigarette Factory, China Tobacco Henan Industrial Company Ltd., Zhengzhou 450000, China

Corresponding author: Guanglu Yang (yangguanglu0@163.com)

This work was supported in part by the National Natural Science Foundation of China under Grant U2004166; and in part by the Key Research, Development and Promotion Special Projects (Science and Technology) of Henan Province under Grant 202102210103.

ABSTRACT Neutral-point clamped (NPC) three-level grid-tied converter is the key power electronic equipment connecting renewable energy and power grid. High temperature and other factors can lead to current sensor failure, control strategy failure, output current distortion, and even lead to the disconnection of renewable energy. To maintain the normal operation of NPC three-level grid-tied converter with current sensor fault, a model predictive fault-tolerant control strategy based on space voltage vector set and fault phase current reconstruction is proposed. Firstly, the relationship between fault phase current and voltage vector is studied. After the current sensor fault, only 12 out of 27 voltage vectors were found to be able to reconstruct faulty phase currents with a DC current sensor and an AC current sensor. Model predictive current control using the set of these 12 voltage vectors, and fault phase current is directly calculated by DC current and normal phase current, which improves the fault tolerance and stability of the converter system. Finally, simulation and experimental results verified the effectiveness of the proposed method.

INDEX TERMS Neutral-point clamped grid-tied converter, model predictive control, current sensor fault, fault-tolerant, current reconstruction.

I. INTRODUCTION

Neutral-point-clamped (NPC) three-level grid-tied converter serves in high-voltage and high-power applications because of its low harmonic content of output current and high conversion efficiency [1]. When the converter system fails, the control strategy will fail, the grid-tied current will be seriously distorted, and the DC power supply will be disconnected. Since the converter works in a high-temperature environment, sensor components made of ferrite may fault [2]–[5]. Therefore, it is significant to study the fault-tolerant of NPC converter with current sensor fault.

Model predictive control (MPC) has been studied because of its simple control strategy, good robustness, and without PWM wave modulation [6]–[11]. Its main feature is using the system model to predict the future changes of control variables. According to the predetermined cost function, the optimal operation mode of the converter is determined. MPC predicts the optimal switching state in the next period by the relationship between the three-phase current signal and voltage feedforward.

Sensor faults can be divided into complete failure fault, fixed deviation fault, drift deviation fault, and accuracy decline. Sensor faults can lead to abnormal operation of the control system, resulting in unpredictable negative consequences. So many scholars have studied the fault-tolerant process of sensor fault [12]–[14]. The residual current sensor can be used to reconstruct the three-phase current and improve the stability of the conversion system, and such strategies are applied in motors and grid-tied converters [15]–[19]. A PWM control strategy using DC-link current to reconstruct the fault phase current is proposed for the two-level converter. According to the DC-link current information under different switching states, all phase currents are reconstructed in a single PWM cycle [18]. However, under some voltage vectors, the DC-link current cannot reconstruct the fault phase current. The voltage vectors are divided into two categories: reconstructing the fault phase current with DC-link current and the fault phase current with predicted current [19]. Although all voltage vectors are used in this strategy, the fault phase

The associate editor coordinating the review of this manuscript and approving it for publication was Shuaihu Li.

current reconstructed by the predicted current will produce the current error.

In addition, observer-based fault-tolerant strategies for current sensors have been widely studied [20]–[22]. An innovative method for estimating three-phase current using DC-link current is proposed [22]. This method is based on a sinusoidal curve fitting observer and uses trigger signal and DC-link current to reconstruct current. Even if the DC-link current cannot reconstruct the fault phase current, this method can reconstruct the fault phase current. The current reconstruction method does not need DC-link current but requires complex observer parameters. Using multiple voltage vector control in one control cycle could obtain different phase current signals, the fault phase current can be reconstructed [23], [24]. After a dead-time, A/D conversion time, and current stability time, DC-link current can be accurately sampled, and multiple samples are required in each cycle. Therefore, there will be an unmeasurable area in the DC-link. Translate the PWM wave of the corresponding phase with the maximum and minimum duty cycle back and forth to meet the time required for accurate sampling [23].

The above current sensor fault researches are mainly applied to the two-level grid-tied converter. The current sensor fault tolerance of the NPC three-level grid-tied converter has not been further studied. A three-level current reconstruction method for NPC is proposed, in which a shunt resistor is inserted at the neutral point to reconstruct fault phase current according to the current of the shunt resistor [25]. However, this method requires additional resistance elements, which is unsuitable for conventional NPC three-level converter and will cause additional power loss. Aiming at the current sensor fault of NPC three-level grid-tied converter, an MPC strategy based on current reconstruction is proposed. The main contributions are summarized as follows:

1. The NPC three-level current reconstruction model is established. When AC current sensor fails, the voltage vector of NPC three-level grid-tied converter is analyzed, and the fault phase current is reconstructed by DC-link current.

2. The current predictive control model is designed based on the reconstructed current, an MPC strategy is proposed. And the neutral voltage component is added to the cost function to balance the capacitor voltage.

3. The proposed MPC strategy has good steady-state performance under different loads and can quickly follow the reference current. It ensures the continuous operation of NPC three-level grid-tied converter after the current sensor fault.

II. CURRENT RECONSTRUCTION MODEL AND CURRENT PREDICTIVE CONTROL MODEL

A. CURRENT RECONSTRUCTION MODEL

The conventional NPC three-level grid-tied converter topology is shown in Fig. 1. Each phase consists of 4 IGBTs and 2 diodes. In addition, the converter system includes a DC power supply $U_{\rm dc}$ and two capacitors. The grid is connected with filter inductor L and parasitic resistor R. Fig. 2 shows the converter voltage vector in the normal state.

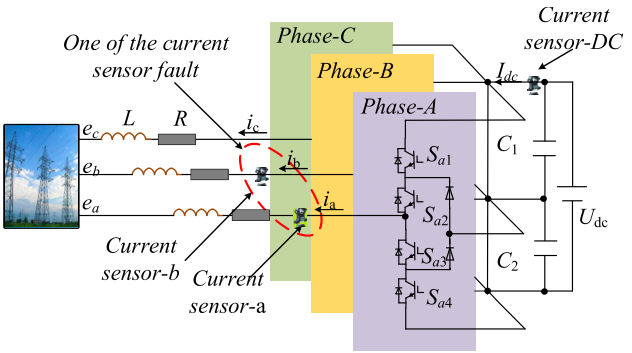

FIGURE 1. Topology of NPC three-level grid-tied converter with current sensor fault.

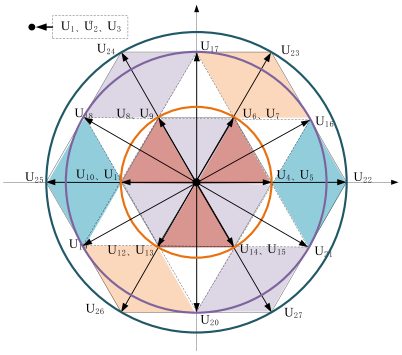

FIGURE 2. NPC three-level voltage vectors in normal state.

Under the normal state, NPC three-level grid-tied converter controller needs to collect real-time signals of three-phase current and three-phase voltage. The three-phase current signals are collected and transmitted by two AC current sensors (Assuming phase a is connected to current sensor-a; phase b is connected to current sensor-b; phase c current can be calculated with Kirchhoff current law). The high temperature and high voltage environment may damage such sensitive devices as the current sensor.

When the current sensor-a fault and the current sensor-b works normally, the phase b current can be directly obtained, while the current phase a current and phase c current are inaccurate. Under this state, phase b current i_b and phase c current i_c need to be reconstructed. When the current sensor-b fails and the current sensor-a works normally, the phase a current can be obtained directly, and phase b current and phase c current are inaccurate. Under this state, phase a current i_a and phase c current i_c need to be reconstructed.

The relationship between DC-link current and three-phase current is (1).

$$\begin{cases} I_{dc} = S_{HA} \times i_a + S_{HB} \times i_b + S_{HC} \times i_c \\ i_a + i_b + i_c = 0 \end{cases} \tag{1}$$

where I_{dc} is DC-link current; i_a, i_b, and i_c are the output three-phase current of the converter system; S_{HA}, S_{HB}, and

S_{HC} are defined as (2):

$$S_{HX} = \begin{cases} 1 & S_X = 1 \\ 0 & others \end{cases} \quad X = A, B, C \tag{2}$$

According to (1), the reconstructed fault phase current can be expressed as (3) and (4):

$$i_a = \begin{cases} \dfrac{I_{dc} - (S_{HB} - S_{HC}) \times i_b}{S_{HA} - S_{HC}}, & S_{HA} - S_{HC} \neq 0 \\ 0, & S_{HA} - S_{HC} = 0 \end{cases} \tag{3}$$

$$i_b = \begin{cases} \dfrac{I_{dc} - (S_{HA} - S_{HC}) \times i_a}{S_{HB} - S_{HC}}, & S_{HB} - S_{HC} \neq 0 \\ 0, & S_{HB} - S_{HC} = 0 \end{cases} \tag{4}$$

After reconstructing phase b current i_b or phase a current i_a, phase c current i_c can be obtained with $i_c = - i_a - i_b$. As shown in Fig. 3, when the current sensor-a fails, i_a can be reconstructed with (3) if $S_{HA} \neq S_{HC}$. The voltage vectors that can be used are $U_4(1, 0, 0)$, $U_6(1, 1, 0)$, $U_{10}(0, 1, 1)$, $U_{12}(0, 0, 1)$, $U_{16}(1, 0, -1)$, $U_{19}(-1, 0, 1)$, $U_{20}(0, -1, 1)$, $U_{21}(1, -1, 0)$, $U_{22}(1, -1, -1)$, $U_{23}(1, 1, -1)$, $U_{25}(-1, 1, 1)$, $U_{26}(-1, -1, 1)$; When the current sensor-b fails, i_b can be reconstructed with (4) if $S_{HB} \neq S_{HC}$. The voltage vectors that can be used are $U_6(1, 1, 0)$, $U_8(0,1,0)$, $U_{12}(0, 0, 1)$, $U_{14}(1, 0, 1)$, $U_{17}(0, 1, -1)$, $U_{18}(-1, 1, 0)$, $U_{19}(-1, 0, 1)$, $U_{20}(0, -1, 1)$, $U_{23}(1, 1, -1)$, $U_{24}(-1, 1, -1)$, $U_{26}(-1, -1, 1)$, $U_{27}(1, -1, 1)$.

TABLE 1. Correspondence relationship between voltage vector and reconstruction current in current sensor-a fault.

Voltage Vector	Phase a Current i_{ar}	Phase b Current i_{br}	Phase c Current i_{cr}
$U_4(1, 0, 0)$	I_{dc}	i_b	$-i_{ar}-i_{br}$
$U_6(1, 1, 0)$	$I_{dc}-i_{br}$	i_b	$-i_{ar}-i_{br}$
$U_{10}(0, 1, 1)$	$-I_{dc}$	i_b	$-i_{ar}-i_{br}$
$U_{12}(0, 0, 1)$	$-I_{dc}-i_{br}$	i_b	$-i_{ar}-i_{br}$
$U_{16}(1, 0, -1)$	I_{dc}	i_b	$-i_{ar}-i_{br}$
$U_{19}(-1, 0, 1)$	$-I_{dc}-i_{br}$	i_b	$-i_{ar}-i_{br}$
$U_{20}(0, -1, 1)$	$-I_{dc}-i_{br}$	i_b	$-i_{ar}-i_{br}$
$U_{21}(1, -1, 0)$	I_{dc}	i_b	$-i_{ar}-i_{br}$
$U_{22}(1, -1, -1)$	I_{dc}	i_b	$-i_{ar}-i_{br}$
$U_{23}(1, 1, -1)$	$I_{dc}-i_{br}$	i_b	$-i_{ar}-i_{br}$
$U_{25}(-1, 1, 1)$	$-I_{dc}$	i_b	$-i_{ar}-i_{br}$
$U_{26}(-1, -1, 1)$	$-I_{dc}-i_{br}$	i_b	$-i_{ar}-i_{br}$

In the current relationship shown in (3) and (4), the three-phase current is obtained by the current reconstruction method, which improves the reliability of the NPC three-level grid-tied system. The current reconstruction model is established with the relationship between DC-link current and normal phase current. In Table 1, the three-phase current can be obtained by DC-link current I_{dc} and phase b current i_b after the current sensor-a fault. As shown in Table 2, the three-phase current can be obtained by using DC-link current I_{dc} and phase a current i_a after the current sensor-b fault.

B. CURRENT PREDICTIVE MODEL

Reconstructed current is applied to the current sensor fault, and the current predictive model is shown in this section.

TABLE 2. Correspondence relationship between voltage vector and reconstruction current in current sensor-b fault.

Voltage Vector	Phase a Current i_{ar}	Phase b Current i_{br}	Phase c Current i_{cr}
$U_6(1, 1, 0)$	i_a	$I_{dc}-i_{ar}$	$-i_{ar}-i_{br}$
$U_8(0, 1, 0)$	i_a	I_{dc}	$-i_{ar}-i_{br}$
$U_{12}(0, 0, 1)$	i_a	$-I_{dc}-i_{ar}$	$-i_{ar}-i_{br}$
$U_{14}(1, 0, 1)$	i_a	$-I_{dc}$	$-i_{ar}-i_{br}$
$U_{17}(0, 1, -1)$	i_a	I_{dc}	$-i_{ar}-i_{br}$
$U_{18}(-1, 1, 0)$	i_a	I_{dc}	$-i_{ar}-i_{br}$
$U_{19}(-1, 0, 1)$	i_a	$-I_{dc}-i_{ar}$	$-i_{ar}-i_{br}$
$U_{20}(0, -1, 1)$	i_a	$-I_{dc}-i_{ar}$	$-i_{ar}-i_{br}$
$U_{23}(1, 1, -1)$	i_a	$I_{dc}-i_{ar}$	$-i_{ar}-i_{br}$
$U_{24}(-1, 1, -1)$	i_a	I_{dc}	$-i_{ar}-i_{br}$
$U_{26}(-1, -1, 1)$	i_a	$-I_{dc}-i_{ar}$	$-i_{ar}-i_{br}$
$U_{27}(1, -1, 1)$	i_a	$-I_{dc}$	$-i_{ar}-i_{br}$

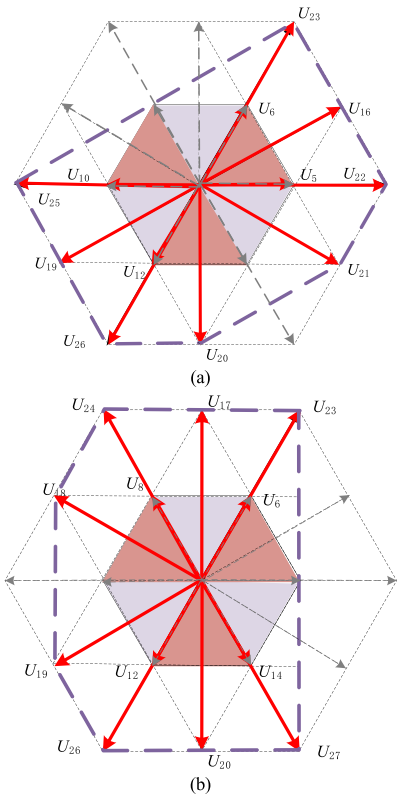

FIGURE 3. Available voltage vectors of the current sensor-a fault and current sensor-b fault: (a) Available voltage vectors in current sensor-a fault; (b) Available voltage vectors in current sensor-b fault.

There are three switching states for each phase, and the switching state of each phase S_i is defined as (5).

$$S_i = \begin{cases} 1 & S_{i1} = on, S_{i2} = on, S_{i3} = off, S_{i4} = off \\ 0 & S_{i1} = on, S_{i2} = off, S_{i3} = off, S_{i4} = on \\ -1 & S_{i1} = off, S_{i2} = off, S_{i3} = on, S_{i4} = on \end{cases} \tag{5}$$

where S_{in} ($i \in \{a, b, c\}$, $n \in \{1, 2, 3, 4\}$) denotes the switch in the main circuit; "*on*" and "*off*" represent that the power switch is turned on and turned off, respectively.

NPC three-level grid-tied converter has 27 switching states, and each switch state corresponds to an output voltage vector.

The output voltage vector u_n can be expressed as (6).

$$u_n = \frac{\sqrt{2}}{\sqrt{3}}\left(u_a e^{j0} + u_b e^{j\frac{2\pi}{3}} + u_c e^{-j\frac{2\pi}{3}}\right) \quad n = 1, \ldots, 27 \tag{6}$$

where u_i ($i \in \{a, b, c\}$) represents the three-phase output voltage, respectively.

In addition, the three-phase output voltage can be expressed as (7).

$$\begin{cases} u_a = \dfrac{U_{dc} S_a}{2} \\ u_b = \dfrac{U_{dc} S_b}{2} \\ u_c = \dfrac{U_{dc} S_c}{2} \end{cases} \tag{7}$$

In $\alpha\beta$ coordinate system, u_a, u_b, u_c can be expressed as (8).

$$\begin{bmatrix} u_\alpha \\ u_\beta \end{bmatrix} = \frac{U_{dc}}{\sqrt{6}} \begin{bmatrix} 1 & -1/2 & -1/2 \\ 0 & \sqrt{3}/2 & -\sqrt{3}/2 \end{bmatrix} \begin{bmatrix} S_a \\ S_b \\ S_c \end{bmatrix} \tag{8}$$

where u_α and u_β are the output voltages of the converter.

According to Fig. 1, the voltage relationship of NPC three-level grid-tied converter can be expressed as (9):

$$\frac{L d\boldsymbol{i}_{\alpha\beta}}{dt} = \boldsymbol{u}_{\alpha\beta}(k) - R\boldsymbol{i}_{\alpha\beta}(k) - \boldsymbol{e}_{\alpha\beta}(k) \tag{9}$$

where T_s is the sampling period. $\boldsymbol{u_{\alpha\beta}}(k) = [u_\alpha(k), u_\beta(k)]^{\mathrm{T}}$, $\boldsymbol{u_{\alpha\beta}}(k)$ is the output voltage at kth instant. $\boldsymbol{i_{ab}}(k) = [i_\alpha(k), i_\beta(k)]^{\mathrm{T}}$, $i_\alpha(k)$ and $i_\beta(k)$ are the output currents at kth instant. $\boldsymbol{e_{\alpha\beta}}(k) = [e_\alpha(k), e_\beta(k)]^{\mathrm{T}}$, $e_\alpha(k)$ and $e_\beta(k)$ are grid voltage at kth instant.

(10) can be deduced with (9).

$$\frac{L[\boldsymbol{i}_{\alpha\beta}(k+1) - \boldsymbol{i}_{\alpha\beta}(k)]}{T_s} = \boldsymbol{u}_{\alpha\beta}(k) - R\boldsymbol{i}_{\alpha\beta}(k) - \boldsymbol{e}_{\alpha\beta}(k) \tag{10}$$

where $\boldsymbol{i_{\alpha\beta}}(k+1) = [i_\alpha(k+1), i_\beta(k+1)]^{\mathrm{T}}$; $i_\alpha(k+1)$and $i_\beta(k+1)$ are the output currents at $(k+1)$th instant.

The current prediction expression at $(k+1)$th instant can be calculated as (11):

$$\boldsymbol{i}_{\alpha\beta}(k+1) = \frac{T_s\,[\boldsymbol{u}_{\alpha\beta}(k) - \boldsymbol{e}_{\alpha\beta}(k)]}{L} + \left(1 - \frac{RT_s}{L}\right)\boldsymbol{i}_{\alpha\beta}(k) \tag{11}$$

III. MODEL PREDICTIVE CONTROL BASED ON CURRENT RECONSTRUCTION

The conventional MPC voltage vector selection is calculated 27 voltage vectors' cost function and select the optimal vector, and 12 calculations are required for each period after the current sensor fails.

To getting the optimal voltage vector, all the predicted currents at $(k+1)$th instant are substituted into the cost function g to evaluate current control errors. The voltage vector that minimizes the cost function (12) will be selected as the optimal vector, which will control the converter at the next instant.

$$g = |i_{\alpha\mathrm{ref}} - i_\alpha(k+1)| + \left|i_{\beta\mathrm{ref}} - i_\beta(k+1)\right| + p\,|\Delta u_{dc}(k+1)| \tag{12}$$

where $i_{\alpha ref}$ and $i_{\beta ref}$ are the reference currents; p is the weight factor of voltage balance; Δu_{dc} is the voltage error of the upper and lower capacitor, as (13).

$$\begin{cases} \Delta u_{dc}(k+1) = \Delta u_{dc}(k) + i_o \\ i_o = \dfrac{T_s(S_{OA} \times i_a + S_{OB} \times i_b + S_{OC} \times i_c)}{C} \end{cases} \tag{13}$$

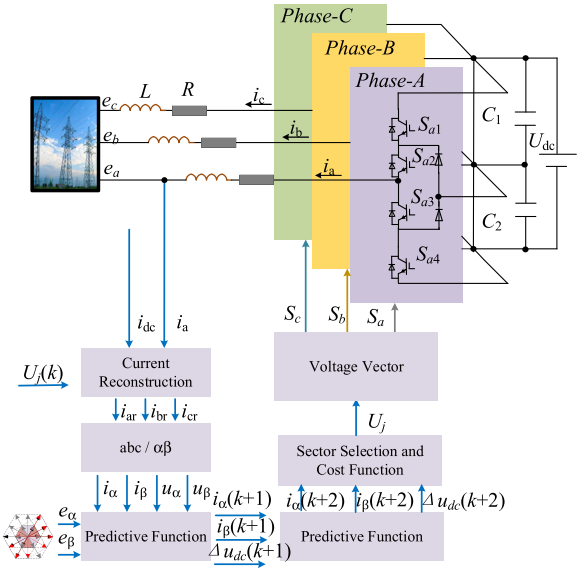

FIGURE 4. Model predictive current control structure based on current reconstruction.

And S_{OX} is defined as (14).

$$S_{OX} = \begin{cases} 1 & S_X = 0 \\ 0 & others \end{cases} \quad X = A, B, C \tag{14}$$

where i_o is neutral point current; C is DC side capacitance.

The selection of the optimal voltage vector takes a lot of time, resulting in a time delay between the optimal voltage vector and the actual voltage vector. Therefore, the time delay is compensated by applying the optimal voltage vector at $(k+2)$th instant, as shown in (15):

$$\boldsymbol{i}_{\alpha\beta}(k+2) = \frac{T_s\,[\boldsymbol{u}_{\alpha\beta}(k+1) - \boldsymbol{e}_{\alpha\beta}(k)]}{L} + \left(1 - \frac{RT_s}{L}\right)\boldsymbol{i}_{\alpha\beta}(k+1) \tag{15}$$

where $\boldsymbol{i_{\alpha\beta}}(k+2) = [i_\alpha(k+2), i_\beta(k+2)]^{\mathrm{T}}$, $i_\alpha(k+2)$and $i_\beta(k+2)$ are the output currents of the converter at $(k+2)$th instant.

The voltage vector which minimizes the cost function (16) is selected as the optimal voltage vector.

$$g = \left|i_{\alpha ref} - i_\alpha(k+2)\right| + \left|i_{\beta ref} - i_\beta(k+2)\right| + p\,|\Delta u_{dc}(k+2)| \tag{16}$$

$$\begin{cases} \Delta u_{dc}(k+2) = \Delta u_{dc}(k+1) + i_o \\ i_o = \dfrac{T_s(S_a \times i_a(k+2) + S_b \times i_b(k+2) + S_b \times i_c(k+2))}{C} \end{cases} \tag{17}$$

MPC structure based on current reconstruction is shown in Fig. 4, and model predictive current flow based on current reconstruction is shown in Fig. 5. The control flow of current reconstruction is as follows:

Step 1: collect grid side voltage $e(k)$, phase a current $i_a(k)$, phase b current $i_b(k)$ and DC-link current $I_{dc}(k)$.

Step 2: collect the optimal voltage vector $U_j(k)$ and converter output voltage $u(k)$.

Step 3: calculation of S_{HA}, S_{HB}, S_{HC}.

Step 4: calculate the reconstructed current i_a or i_b.

Step 5: reconstruct phase c current $i_c(k)$.

Step 6: calculate converter output voltage $u(k+1)$, $u(k+2)$.

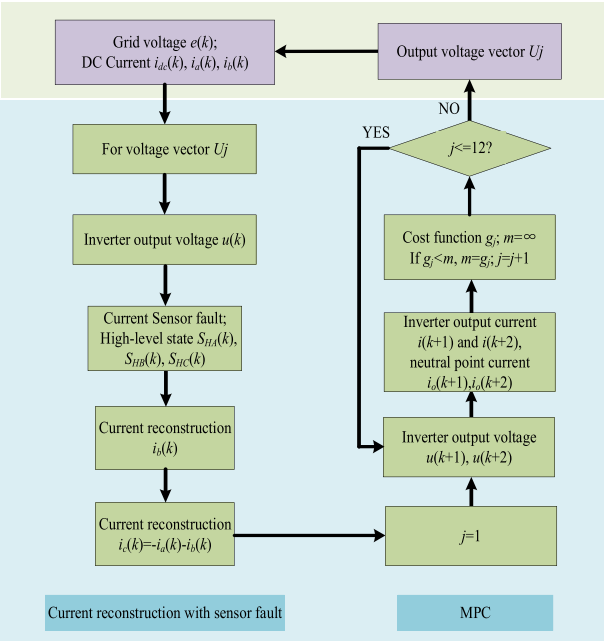

FIGURE 5. Flow chart of model predictive current control based on current reconstruction.

Step 7: calculation of neutral point current $i_o(k+1)$, $i_o(k+2)$ and predicted current $i(k+1)$, $i(k+2)$.

Step 8: calculate the cost function g and select the optimal voltage vector.

TABLE 3. Simulation and experiment parameters.

Symbol	Parameters	Values
U_{dc}	DC voltage	700 V
e	RMS of grid phase voltage	110 V
L	Filter inductance	20 mH
R	Parasitic resistance	0.05 Ω
f	Grid frequency	50 Hz
fs	Sampling frequency	20 kHz

IV. SIMULATION VERIFICATION

In order to verify the effectiveness of the proposed strategy, the dynamic and static simulation is carried out by taking the current sensor-b fault as an example. The parameters used in the simulation system are shown in Table 3.

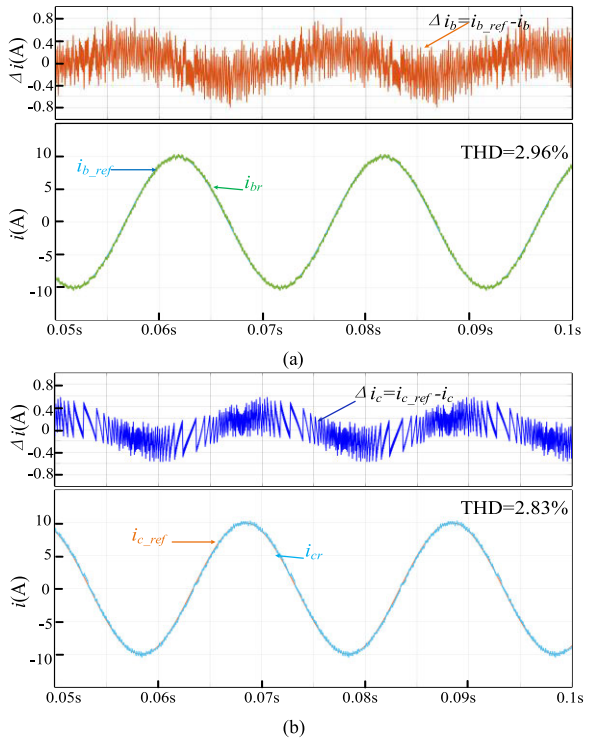

FIGURE 6. Reconstruction current and reference current: (a) Phase b reference current i_{b_ref} and reconstruction current i_{br}; (b) Phase c reference current i_{c_ref} and reconstruction current i_{cr}.

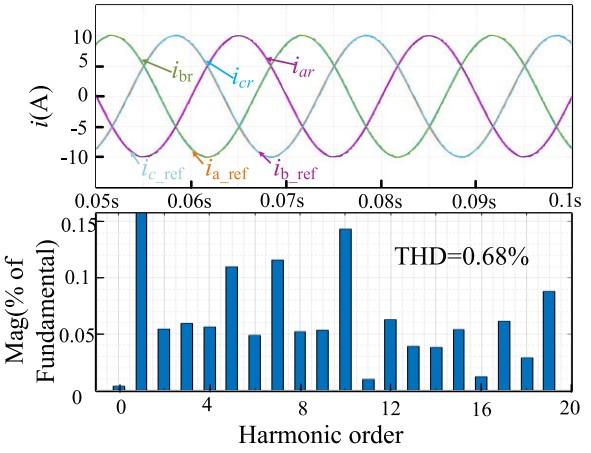

FIGURE 7. Three-phase current under normal state.

A. STEADY-STATE SIMULATION RESULTS

Fig. 6 is the simulation waveform of the reconstruction current i_{br}, i_{cr} and the reference current i_{b_ref}, i_{c_ref} and their current error Δi. In Fig. 6(a), the reconstructed phase b current i_{br} can follow with the reference phase b current i_{b_ref}, and the maximum current error Δi_b is 0.8A. In Fig. 6(b), the reconstructed phase c current i_{cr} can keep up with the reference phase c current i_{c_ref}, and the maximum current

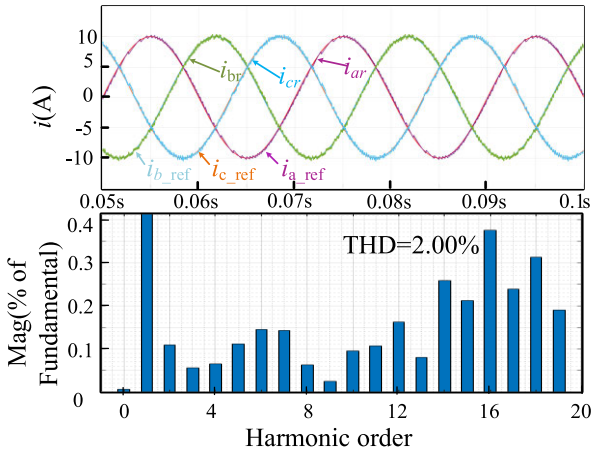

FIGURE 8. Reconstruction current after the current sensor-b fault.

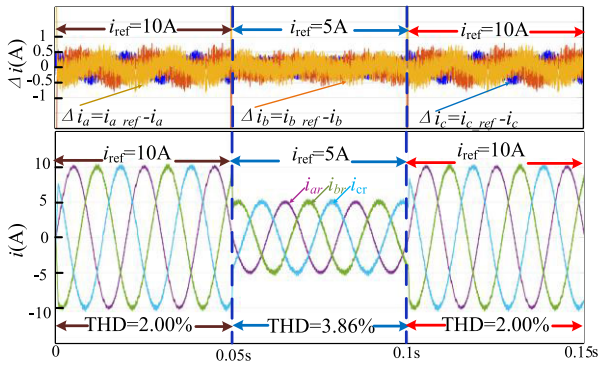

FIGURE 9. Dynamic current after the current sensor-b fault.

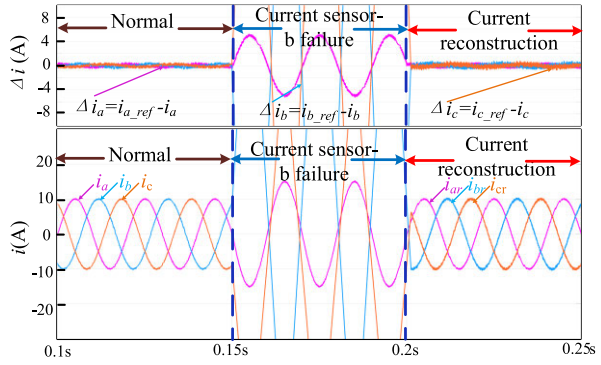

FIGURE 10. Comparison before and after current reconstruction.

error Δi_c is 0.6A. When the reference current i_{ref} =10A, the reconstructed phase b current i_{br} and phase c current i_{cr} can follow with the reference current. And the current error is less than 0.8A, which verifies the effectiveness of the proposed method.

Fig. 7 is the grid side output current waveform i_a, i_b, i_c before the current sensor-b fault, and Fig. 8 is the reconstructed grid side output current waveform i_{ar}, i_{br}, i_{cr} after the current sensor-b fault. Under the normal state, the three-phase current's total harmonic distortion (THD) is 0.68 %. After the current sensor-b fault, the reconstructed three-phase current THD is 2.00 %. Compared with the current under normal state, the reconstructed three-phase current THD increases by 1.32 %.

B. DYNAMIC SIMULATION RESULTS

To verify the dynamic performance of the proposed strategy, Fig. 9 shows the initial reference current i_{ref} =10A, and the reference current drops to 5A at 0.05s; then, the reference current rises to 10A at 0.1s. In Fig. 9, when the reference current is changed from 10A to 5A, the reconstructed three-phase current can keep up with the reference current, and the three-phase current error is reduced by 0.2A. When the reference current changes from 5A to 10A, the reconstructed three-phase current can keep up with the reference current, and the three-phase current error increases by 0.2A.

Given reference current i_{ref} =10A, the dynamic current waveforms under normal state, current sensor-b fault state, and current reconstruction state are shown in Fig. 10. Within 0.1s∼0.15s, the converter works normally; within 0.15s∼0.2s, the current sensor-b fails; within 0.2∼0.25s, the current is reconstructed with the proposed strategy. After the current sensor-b fault, the three-phase current changes malignant and cannot meet the requirements of the grid (To show the effect of the reconstructed current, the peak value of the three-phase current after the current sensor-b fault is not fully showed). After the current reconstruction, the gird current returns to normal. The validity and fault-tolerance of the proposed MPC strategy based on current reconstruction are verified.

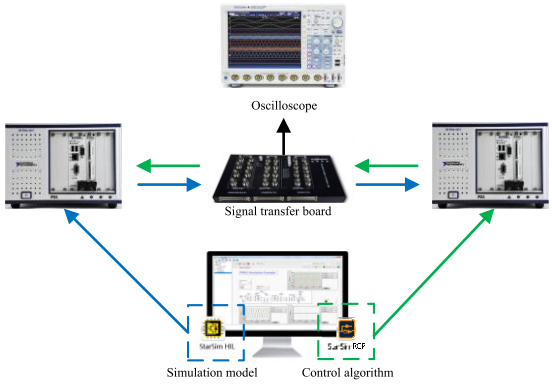

FIGURE 11. Hardware in the loop experimental platform.

Table 4 summarizes the comparison with previous control strategies aimed at the fault phase current reconstruction. A control strategy of reconstructing fault phase current with DC-link current i_{dc} and predictive current $i_b(k)$ is proposed. However, the fault phase current reconstructed by the predicted current will lead to current reconstruction error. A method of inserting single parallel resistance of inverter and reconstructing fault phase current by using parallel resistance current is proposed. Although the current of a parallel resistor can reconstruct a three-phase current, it is not suitable for a conventional NPC three-level converter. Moreover,

TABLE 4. Comparison of effects of different current reconstruction methods on grid-tied system.

	Method A[13]	Method B[19]	Proposed strategy
Reconstructing current signals	DC-link current i_{dc} and predictive current $i_b(k)$	Current from the shunt resistor $i_{abc\_shunt}(k)$	DC-link current i_{dc}
Additional components	No	Single shunt resistor	No
Incremental losses	No	Yes	No
Theoretical reconstruction current error	Yes	No	No
Suitable for conventional NPC	No	No	Yes

the neutral-point current flowing through the resistance will reduce the efficiency of the conversion system. Compared with these two methods, the proposed strategy does not produce current reconstruction error or additional power loss and is suitable for conventional NPC three-level structure.

V. EXPERIMENT VERIFICATION

Build the hardware in the loop experimental platform to verify the proposed strategy, as shown in Fig. 11. The platform uses PXIe-1071 of NI company as a hardware circuit and controller. The test instrument is the Yokogawa DLM4000 oscilloscope, and the sampling frequency is 10kHz.

A. STEADY-STATE EXPERIMENTAL RESULTS

To verifying the validity of the proposed current reconstruction strategy, the steady-state control performance is tested and compared with the conventional NPC three-level grid-tied strategy. When the reference current is 12A, Fig. 12 shows the three-phase current and fast Fourier transformation analysis results under the current sensor-b fault state and current reconstruction state.

In Fig. 12, when the reference current is 12 A, the three-phase current THD under the current sensor-b fault state is 12.25%, while the current THD under the current reconstruction state is 3.39%. The error between reference current and reconstruction current is less than 1A. By comparison, it can be concluded that the proposed strategy can solve the problems caused by the current sensor fault because the DC-link current and the normal phase current can reconstruct the fault phase current.

B. DYNAMIC EXPERIMENTAL RESULTS

Dynamic experiments further verify the performance of the proposed strategy. Fig. 13(a) shows the dynamic three-phase current waveform when the reference current changes from 12A to 10A. Fig. 13(b) shows the dynamic three-phase current waveform when the reference current changes from 10A to 12A.

In Fig. 13, the proposed strategy can follow the reference current regardless of whether the reference current increases or decreases. When the reference current amplitude changes,

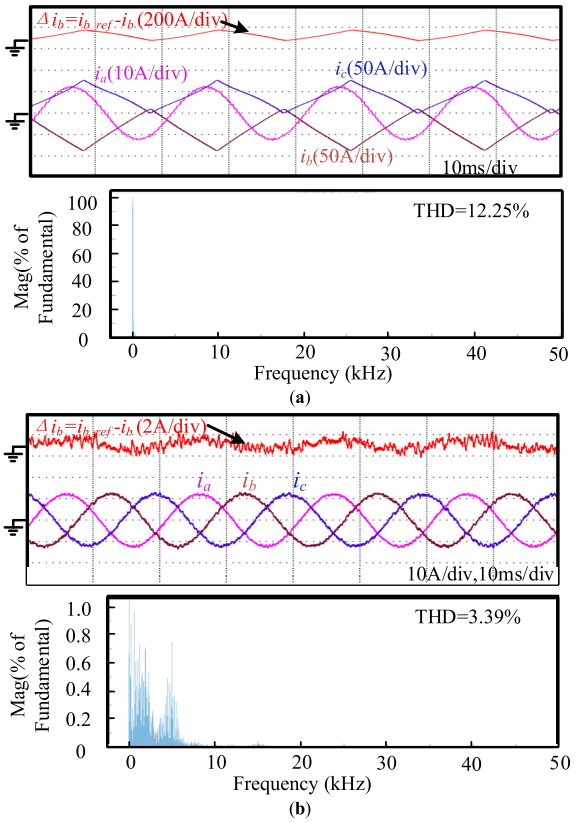

FIGURE 12. Steady-state experimental results of current sensor-b fault when the reference current is 12A: (a) Three-phase current after current sensor-b fault; (b) Three-phase current reconstruction after current sensor-b fault.

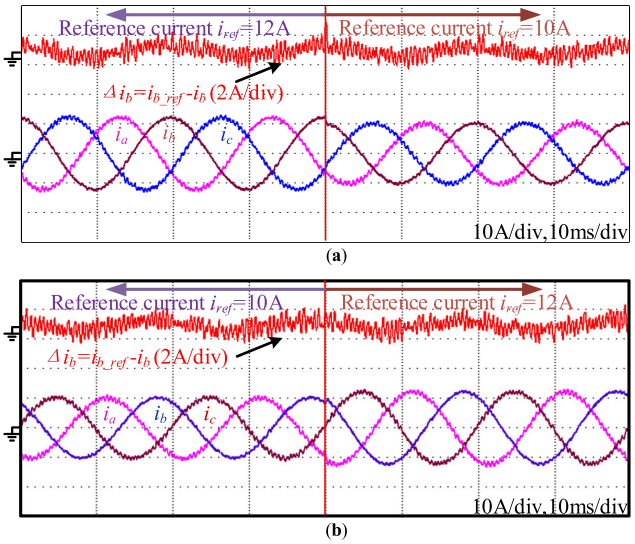

FIGURE 13. Dynamic experimental results of current reconstruction after current sensor-b fault: (a) The reconstructed three-phase current decreases from 12A to 10A; (b) The reconstructed three-phase current rises from 10A to 12A.

the reconstructed three-phase current error is less than 1A. The proposed method can perform fault-tolerant control only with 12 voltage vectors after the current sensor fault.

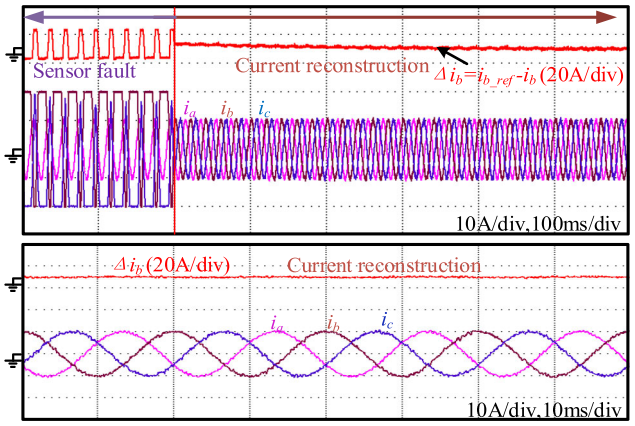

FIGURE 14. Comparison before and after current reconstruction.

Fig. 14 shows the dynamic control process of the proposed MPC strategy after the current sensor-b fails. After the current sensor-b fails, the three-phase current changes seriously and cannot be connected to the grid. After current reconstruction, the three-phase current obviously returns to the normal working state, which further verifies the effectiveness of the proposed method.

VI. CONCLUSION

The controller of NPC three-level grid-tied converter needs the grid side current signal. Once the current sensor fails, the current generated by the converter will significantly impact the grid. An MPC strategy based on current reconstruction is proposed to ensure the NPC three-level grid-tied converter's continuous operation after the current sensor fault. Simulation and experimental platforms are built, and the performance of the proposed control method is tested.

1. The relationship among DC-link current, AC current and voltage vector is analyzed. After the current sensor fault, the voltage vector set comprises voltage vectors directly related to fault phase current. Fault phase current is calculated by DC-link current and normal phase current.

2. A current predictive control model based on voltage vector set and current reconstruction is designed. And MPC current based on current reconstruction for NPC three-level grid-tied converter is proposed, and the cost function selects the optimal voltage vector.

3. Simulation and experimental results show that the proposed strategy can adjust the reconstructed current with the voltage vector set after the current sensor fault. The control strategy improves the continuous operation ability and fault tolerance of NPC three-level grid-tied converter.

REFERENCES

[1] N. El Ouanjli, A. Derouich, A. El Ghzizal, M. Taoussi, Y. El Mourabit, K. Mezioui, and B. Bossoufi, "Direct torque control of doubly fed induction motor using three-level NPC inverter," *Protection Control Mod. Power Syst.*, vol. 4, no. 1, pp. 196–204, Oct. 2019.

[2] T. Muhammed and R. A. Shaikh, "An analysis of fault detection strategies in wireless sensor networks," *J. Netw. Comput. Appl.*, vol. 78, pp. 267–287, Jan. 2017.

[3] N. ElHady and J. Provost, "A systematic survey on sensor failure detection and fault-tolerance in ambient assisted living," *Sensors*, vol. 18, no. 7, p. 1991, Jun. 2018.

[4] Y. Wu and Y. Wu, "Modelling and simulation of sensor fault-tolerant networked control system with uncertainties," *Int. J. Comput. Appl. Technol.*, vol. 56, no. 3, pp. 210–218, 2017.

[5] N. E. ElHady, S. Jonas, J. Provost, and V. Senner, "Sensor failure detection in ambient assisted living using association rule mining," *Sensors*, vol. 20, no. 23, p. 6760, Nov. 2020.

[6] L. Guo, N. Jin, C. Gan, and K. Luo, "Hybrid voltage vector preselection-based model predictive control for two-level voltage source inverters to reduce the common-mode voltage," *IEEE Trans. Ind. Electron.*, vol. 67, no. 6, pp. 4680–4691, Jun. 2020.

[7] N. Vafamand, M. H. Khooban, T. Dragičević, and F. Blaabjerg, "Networked fuzzy predictive control of power buffers for dynamic stabilization of DC microgrids," *IEEE Trans. Ind. Electron.*, vol. 66, no. 2, pp. 1356–1362, Feb. 2019.

[8] S. Vazquez, J. Rodriguez, M. Rivera, L. G. Franquelo, and M. Norambuena, "Model predictive control for power converters and drives: Advances and trends," *IEEE Trans. Ind. Electron.*, vol. 64, no. 2, pp. 935–947, Feb. 2017.

[9] Y. Xia, B. Gou, and Y. Xu, "A new ensemble-based classifier for IGBT open-circuit fault diagnosis in three-phase PWM converter," *Protection Control Mod. Power Syst.*, vol. 3, no. 1, pp. 364–372, Nov. 2018.

[10] L. Guo, N. Jin, Y. Li, and K. Luo, "A model predictive control method for grid-connected power converters without AC voltage sensors," *IEEE Trans. Ind. Electron.*, vol. 68, no. 2, pp. 1299–1310, Feb. 2021.

[11] X. Zhang, B. Hou, and Y. Mei, "Deadbeat predictive current control of permanent-magnet synchronous motors with stator current and disturbance observer," *IEEE Trans. Power Electron.*, vol. 32, no. 5, pp. 3818–3834, May 2017.

[12] J. Lu, X. Zhang, Y. Hu, J. Liu, C. Gan, and Z. Wang, "Independent phase current reconstruction strategy for IPMSM sensorless control without using null switching states," *IEEE Trans. Ind. Electron.*, vol. 65, no. 6, pp. 4492–4502, Jun. 2018.

[13] Q. Sun, J. Wu, C. Gan, Y. Hu, N. Jin, and J. Guo, "A new phase current reconstruction scheme for four-phase SRM drives using improved converter topology without voltage penalty," *IEEE Trans. Ind. Electron.*, vol. 65, no. 1, pp. 133–144, Jan. 2018.

[14] C. Gan, J. Wu, S. Yang, and Y. Hu, "Phase current reconstruction of switched reluctance motors from DC-link current under double high-frequency pulses injection," *IEEE Trans. Ind. Electron.*, vol. 62, no. 5, pp. 3265–3276, May 2015.

[15] Y. Xu, H. Yan, J. Zou, B. Wang, and Y. Li, "Zero voltage vector sampling method for PMSM three-phase current reconstruction using single current sensor," *IEEE Trans. Power Electron.*, vol. 32, no. 5, pp. 3797–3807, Jul. 2017.

[16] S. Song, Z. Xia, G. Fang, R. Ma, and W. Liu, "Phase current reconstruction and control of three-phase switched reluctance machine with modular power converter using single DC-link current sensor," *IEEE Trans. Power Electron.*, vol. 33, no. 10, pp. 8637–8649, Oct. 2018.

[17] H. Lu, X. Cheng, W. Qu, S. Sheng, Y. Li, and Z. Wang, "A three-phase current reconstruction technique using single DC current sensor based on TSPWM," *IEEE Trans. Power Electron.*, vol. 29, no. 3, pp. 1542–1550, Mar. 2014.

[18] Y.-J. Lee, Y. Cho, and G.-H. Choe, "A phase current reconstruction technique using a single current sensor for interleaved three-phase bidirectional converters," *J. Electr. Eng. Technol.*, vol. 11, no. 4, pp. 905–914, Jul. 2016.

[19] N. Jin, C. Pan, Y. Li, S. Hu, and J. Fang, "Model predictive control for virtual synchronous generator with improved vector selection and reconstructed current," *Energies*, vol. 13, no. 20, p. 5435, Oct. 2020.

[20] Y. Li, W. Li, L. Guo, N. Jin, and F. Lu, "Current sensor-less virtual synchronous generator model predictive control based on sliding mode observer," *IEEE Access*, vol. 9, pp. 17898–17908, 2021.

[21] C. Zhang, H. Liao, X. Li, J. Sun, and J. He, "Fault reconstruction based on sliding mode observer for current sensors of PMSM," *J. Sensors*, vol. 2016, Nov. 2016, Art. no. 9307560.

[22] B. Saritha and P. A. Janakiraman, "Sinusoidal three-phase current reconstruction and control using a DC-link current sensor and a curve-fitting observer," *IEEE Trans. Ind. Electron.*, vol. 54, no. 5, pp. 2657–2664, Oct. 2007.
[23] C. Jianbo, H. Yuwen, and H. Wenxin, "Phase current sampling reconstruction for inverter," *Trans. China Electrotech. Soc.*, vol. 25, no. 4, pp. 111–117, Jan. 2010.
[24] Y. P. Shen, Z. F. Zheng, and X. L. Yang, "A compatible SVPWM method for DC bus current sampling," *Trans. China Electrotech. Soc.*, vol. 36, no. 8, pp. 1617–1627, Apr. 2021.
[25] F. Xu, S. Olaru, V. Puig, C. Ocampo-Martinez, and S.-I. Niculescu, "Sensor-fault tolerance using robust MPC with set-based state estimation and active fault isolation," *Int. J. Robust Nonlinear Control*, vol. 27, no. 8, pp. 1260–1283, May 2017.

HUI LI was born in Shandong, China, in 1980. She received the master's degree in pattern recognition and intelligent system from Zhengzhou University, Zhengzhou, China, in 2007. She is currently a Lecturer at Zhengzhou University of Light Industry. Her research interest includes model predictive control for grid-tied power converters.

HAN XIAO was born in Hebi, China, in 1996. He received the B.S. degree in electrical engineering from Zhengzhou University of Light Industry, Zhengzhou, China, in 2019, where he is currently pursuing the master's degree. His research interest includes model predictive control for power converters.

GUANGLU YANG was born in Henan, China, in 1979. He received the B.S. degree in electrical engineering from Zhengzhou University of Light Industry, Zhengzhou, China, in 2001. He is currently a Senior Engineer at Nanyang Cigarette Factory, China Tobacco Henan Industrial Company Ltd., and a Master Supervisor with Zhengzhou University of Light Industry. His research interests include model predictive control for power converters and tolerant control of power electronics systems.